



Supporting Online Material for

Antennal Mechanosensors Mediate Flight Control in Moths

Sanjay P. Sane,* Alexandre Dieudonné, Mark A. Willis, Thomas L. Daniel

*To whom correspondence should be addressed. E-mail: sane@u.washington.edu

Published 9 February 2007, *Science* **315**, 863 (2007)
DOI: 10.1126/science.1133598

This PDF file includes:

Materials and Methods
Figs. S1 to S5

Other Supporting Online Material for this manuscript includes the following:
(available at www.sciencemag.org/cgi/content/full/315/5813/863/DC1)

Movies S1 to S3

Supplementary Information

Antennal mechanosensors mediate flight control in Lepidoptera

S.P. Sane*, A. Dieudonne, M.A. Willis and T.L. Daniel

*To whom correspondence should be addressed email: sane@u.washington.edu

Contents

Materials and Methods

- S1) High-speed filming of antennal movement.
- S2) Magnitudes of Coriolis torques relative to aerodynamic torques on moth antennae.
- S3) Derivation of frequency characteristics of Coriolis forces on a vibrating antenna.
- S4) Neurophysiology of antennal mechanosensors.
- S5) Measurement of free flight behavior of moths with intact vs. amputated flagella.

Supplementary Video

Supplementary Movies of free flight experiments for moths with:

- S6) Intact flagella
- S7) Removed flagella
- S8) Flagella reattached with glue

Materials and Methods

S1: High-Speed filming of antennal movement in hovering *Manduca sexta*.

Three orthogonally placed high-speed digital video cameras (Photron APX, San Diego, CA) were used to film freely flying hawk moths while the moths tracked an artificial flower moving back-and-forth at 0.5 Hz. The moth was filmed at a resolution of 1024 X 1024 pixels at 500 fps. This video frame rate was approximately 20 times the wing beat frequency. The tip and base of the antennae were digitized in each frame using a custom code written by Dr. T.L. Hedrick in MATLAB (The Mathworks Inc., Natick, NJ). The three-camera configuration allowed us to determine the three-dimensional motion of the antennal tip with respect to the base. The digitization error, determined by calculating the variation in distance between the bases of the two antennae was about 0.37 mm, less than 2% of the antennal length (*ca.* 20 mm). The antennae vibrated regularly in all 5 high speed sequences. Of these, we digitized two sequences (4 antennae, *ca.* 2000 frames per antenna) and both showed similar results. Hence, values from only one sequence have been used in this paper. We measured the lengths of the left ($0.0208 \text{ m} \pm 0.00061 \text{ m}$) and right ($0.0213 \pm 0.00062 \text{ m}$) antennae as function of time. The change in antennal length (approx. 2.9%) is well within measurement error. The antennae were held at constant inter-antennal angles of $143 \pm 3^\circ$.

S2: Estimates of Coriolis and aerodynamic torques on moth antennae.

Estimation of torques due to aerodynamic forces on the antennae

The aerodynamic torque due to an element δl at the distance l from the base of the antenna of diameter r is given by

$$\delta T_D = \delta F_D l \quad (\text{S2. 1})$$

where

$$\delta F_D = \frac{1}{2} C_D \rho V^2 r \delta l \quad (\text{S2. 2})$$

Here, $r \delta l$ is an element of the frontal (or cross sectional) area. In equation S2.2, the coefficient of drag (based on frontal area) on an ideal cylinder placed in uniform flow varies with Reynolds number and is given by an empirical equation

$$C_D = 1 + 10(Re)^{-\frac{2}{3}} \quad (\text{S2.3})$$

where $Re = Vc / \nu$ where V is the air speed, c is a characteristic length scale and ν is the kinematic viscosity of air ($1.5 \times 10^{-5} \text{ m}^2/\text{s}$; 1, 2). Integrating equation (S2.1) over the length of the antenna L , we get

$$T_D = \int_0^L \delta F_D l = \int_0^L \frac{1}{2} C_D \rho V^2 r l \delta l = \frac{1}{2} C_D \rho V^2 r \frac{L^2}{2} \quad (\text{S2.4})$$

For a hovering hawk moth, the measured airspeed due to induced flow was 0.25 m/s. The choice of characteristic length c depends on the scales relevant to the phenomena under investigation. Due to antennal vibrations and *non-uniform* flow field along the antennal length, the typical natural flows encountered by an antenna are not constant but fluctuate. Based on the assumption of a 0.3 mm thin cylinder placed in a *uniform* flow field of 0.25 m/s, we conservatively estimated the Reynolds number value to be approximately 5. When substituted in equation (S2.3), we obtained a drag coefficient of 4.4 for a hawk moth antenna in uniform flow.

Using these values ($C_D=4.4$, $\rho=1.25 \text{ kg/m}^3$, $V=0.25 \text{ m/s}$, $r = 0.3 \text{ mm}$, $L=20\text{mm}$), the aerodynamic torque on the base of the antenna $T_D=1.03 \times 10^{-8} \text{ N-m}$. Similarly, for

$V=0.5$ m/s, $C_D=3.2$ and thus $T_D=3 \times 10^{-8}$ N-m and for $V=1$ m/s, $C_D=2.4$ and $T_D=9 \times 10^{-8}$ N-m.

Estimation of torques due to Coriolis forces on the antenna

The Coriolis torque (T_C) due to an element δl at the distance l from the base of an antenna of diameter r is

$$\delta T_C = \delta F_C l \quad (\text{S2.5})$$

where

$$\delta F_C = 2M' \delta l \omega_{body} \omega_{antenna} l \quad (\text{S2.6})$$

In this equation, M' is the mass per unit length of the antenna, ω_{body} is the angular velocity of the moth's body during turns and $\omega_{antenna}$ is the angular velocity of the antenna.

Integrating this equation over the length of the antenna,

$$T_C = \int_0^L \delta F_C l = \int_0^L 2M' \omega_{body} \omega_{antenna} l^2 \delta l \quad (\text{S2.7})$$

Thus,
$$T_C = 2M' \omega_{body} \omega_{antenna} \frac{L^3}{3} \quad (\text{S2.8})$$

Because the total mass of antenna $M = M' L$,

$$T_C = \frac{2}{3} M \omega_{body} \omega_{antenna} L^2 \quad (\text{S2.9})$$

From actual measurements on freely flying moths tracking a plume, we calculated the body angular velocity to be 5 rad/s during typical turns. These values represent moths performing relatively gentler turns during casting flight while odor tracking. Their turns during hovering or immediately following flight initiation from a vertical wall may be much higher in magnitude. From Fourier transforms of the antennal motion (Fig 1E), the

angular amplitude ($\bar{\theta}$) is 0.012 radians at the vibration frequency of 27 Hz corresponding to the wing beat frequency (n). This corresponds to a wave component

$$\theta(t) = \bar{\theta} \sin(2\pi n t) \quad (\text{S2.10})$$

Thus the peak angular velocity of the antenna, given by the first derivative of the above equation, is

$$\dot{\theta}(t) = 2\pi n \bar{\theta} \cos(2\pi n t) \quad (\text{S2.11})$$

and the average angular velocity is given by

$$\bar{\dot{\theta}} = 4n\bar{\theta} \quad (\text{S2.12})$$

From the above equations, the peak magnitude of the angular velocity of the antenna is estimated to be approximately 2 rad/s, whereas the average angular velocity was 1.3 rad/s. The amplitude $\bar{\theta}$ of the antennal vibration is 0.012 radians and wing beat frequency n is 27 Hz. The mass of the male antenna $M=6 \times 10^{-6}$ Kg and antennal length $L=20$ mm. Using these values, we estimated the peak T_C to be approximately equal to 1.63×10^{-8} N-m, whereas average T_C to be approximately equal to 1.04×10^{-8} N-m.

These values indicate that even by a conservative estimation Coriolis torques are of the same order of magnitude as the aerodynamic torques thereby suggesting that there may be instances during the moth's flight when aerodynamic torques exceed Coriolis torques (e.g. during straight fast forward flight) and other instances when Coriolis forces exceed aerodynamic forces (e.g. during sharp turns).

S3: Derivation of the frequency characteristics of Coriolis forces on a vibrating insect antenna during aerial maneuvers

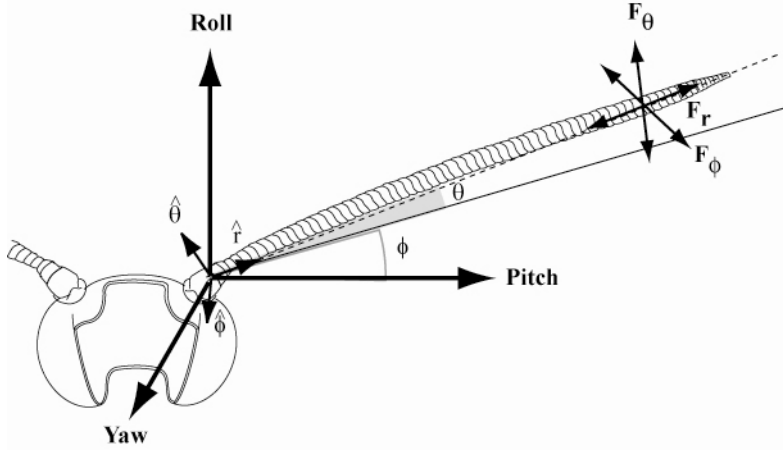


Figure S1: Spherical coordinate system for calculation of Coriolis forces on the antennae of moths (dorsal view).

Consider a spherical coordinate system $(\hat{r}, \hat{\theta}, \hat{\phi})$ centered at the base of the antenna with the unit vector \hat{r} directed along the length of the antenna and $\hat{\theta}, \hat{\phi}$ are the elevation and azimuthal angles respectively (Fig S1). Thus,

$$\vec{r} = r\hat{r} \tag{S3.1}$$

$$\text{and } \dot{\vec{r}} = r\dot{\hat{r}} + \dot{r}\hat{r} \tag{S3.2}$$

where $\vec{}$ denotes vector quantities, $\hat{}$ denotes unit vectors and $\dot{}$ denotes the temporal derivative of the associated variables. In a body-centered coordinate system, Pitch, Roll and Yaw (or *PRY*) denotes body rotations about three mutually orthogonal axes. The origins of the *PRY* and spherical coordinate systems match, such that

$$r\hat{r} = P\hat{P} + R\hat{R} + Y\hat{Y} \tag{S3.3a}$$

$$\text{where, } P = r\text{Cos}\theta\text{Cos}\phi \tag{S3.3b}$$

$$R = r\text{Cos}\theta\text{Sin}\phi \tag{S3.3c}$$

$$\text{and } Y = r\text{Sin}\theta \tag{S3.3d}$$

Substituting Equations S3.3c-d in equation S3.3a,

$$\hat{\mathbf{r}}(\theta, \phi) = (\cos \theta \cos \phi) \hat{\mathbf{P}} + (\cos \theta \sin \phi) \hat{\mathbf{R}} + (\sin \theta) \hat{\mathbf{Y}} \quad (\text{S3.4a})$$

$$\hat{\boldsymbol{\theta}} = \hat{\mathbf{r}}(\theta + \frac{\pi}{2}, \phi) = (-\sin \theta \cos \phi) \hat{\mathbf{P}} + (-\sin \theta \sin \phi) \hat{\mathbf{R}} + (\cos \theta) \hat{\mathbf{Y}} \quad (\text{S3.4b})$$

$$\hat{\boldsymbol{\phi}} = \hat{\mathbf{r}}(\theta = 0, \phi - \frac{\pi}{2}) = (\sin \phi) \hat{\mathbf{P}} + (-\cos \phi) \hat{\mathbf{R}} \quad (\text{S3.4c})$$

Inversely,

$$\hat{\mathbf{P}} = (\cos \theta \cos \phi) \hat{\mathbf{r}} + (-\sin \theta \cos \phi) \hat{\boldsymbol{\theta}} + (\sin \phi) \hat{\boldsymbol{\phi}} \quad (\text{S3.5a})$$

$$\hat{\mathbf{R}} = (\cos \theta \sin \phi) \hat{\mathbf{r}} + (-\sin \theta \sin \phi) \hat{\boldsymbol{\theta}} + (-\cos \phi) \hat{\boldsymbol{\phi}} \quad (\text{S3.5b})$$

$$\hat{\mathbf{Y}} = (\sin \theta) \hat{\mathbf{r}} + (\cos \theta) \hat{\boldsymbol{\theta}} \quad (\text{S3.5c})$$

Thus, from Equation S3.4a

$$\dot{\hat{\mathbf{r}}} = (-\dot{\theta} \sin \theta \cos \phi - \dot{\phi} \cos \theta \sin \phi) \hat{\mathbf{P}} + (-\dot{\theta} \sin \theta \sin \phi + \dot{\phi} \cos \theta \cos \phi) \hat{\mathbf{R}} + (\dot{\theta} \cos \theta) \hat{\mathbf{Y}} \quad (\text{S3.6})$$

Substituting in Equation S3.2, the velocity of the antenna ($\dot{\hat{\mathbf{r}}}$), denoted by $\vec{\mathbf{v}}_{PRY}$ in the PRY system, is given by

$$\begin{aligned} \vec{\mathbf{v}}_{PRY} = \dot{\hat{\mathbf{r}}} = & (\dot{r} \cos \theta \cos \phi - r \dot{\theta} \sin \theta \cos \phi - r \dot{\phi} \cos \theta \sin \phi) \hat{\mathbf{P}} \\ & + (\dot{r} \cos \theta \sin \phi - r \dot{\theta} \sin \theta \sin \phi + r \dot{\phi} \cos \theta \cos \phi) \hat{\mathbf{R}} \\ & + (\dot{r} \sin \theta + r \dot{\theta} \cos \theta) \hat{\mathbf{Y}} \end{aligned} \quad (\text{S3.7})$$

Coriolis terms

The Coriolis forces are given by $\vec{\mathbf{F}}_{coriolis} = 2m\vec{\boldsymbol{\omega}} \times \vec{\mathbf{v}}_{PRY}$ where $\vec{\boldsymbol{\omega}}$ is the angular velocity of the PRY system. If ω_p , ω_R , and ω_y are pitch, roll and yaw angular velocities respectively, then the coriolis forces in the PRY system due to these rotation can be calculated as follows: Consider, for example, a pure pitch rotation given by

$$\vec{\omega} = \omega_p \hat{\mathbf{P}} \quad (\text{S3.8})$$

Thus,

$$\begin{aligned} \vec{\mathbf{F}}_{\text{coriolis}} = 2m(\omega_p \hat{\mathbf{P}}) \times [& (\dot{r} \text{Cos}\theta \text{Cos}\phi - r\dot{\theta} \text{Sin}\theta \text{Cos}\phi - r\dot{\phi} \text{Cos}\theta \text{Sin}\phi) \hat{\mathbf{P}} \\ & + (\dot{r} \text{Cos}\theta \text{Sin}\phi - r\dot{\theta} \text{Sin}\theta \text{Sin}\phi + r\dot{\phi} \text{Cos}\theta \text{Cos}\phi) \hat{\mathbf{R}} \\ & + (\dot{r} \text{Sin}\theta + r\dot{\theta} \text{Cos}\theta) \hat{\mathbf{Y}}] \end{aligned} \quad (\text{S3.9})$$

Substituting $\hat{\mathbf{P}} \times \hat{\mathbf{P}} = 0$, $\hat{\mathbf{P}} \times \hat{\mathbf{R}} = \hat{\mathbf{Y}}$ and $\hat{\mathbf{P}} \times \hat{\mathbf{Y}} = -\hat{\mathbf{R}}$, we get the Coriolis terms:

$$\vec{\mathbf{F}}_{\text{Pitch}} = 2m\omega_p (\dot{r} \text{Cos}\theta \text{Sin}\phi - r\dot{\theta} \text{Sin}\theta \text{Sin}\phi + r\dot{\phi} \text{Cos}\theta \text{Cos}\phi) \hat{\mathbf{Y}} - 2m\omega_p (\dot{r} \text{Sin}\theta + r\dot{\theta} \text{Cos}\theta) \hat{\mathbf{R}} \quad (\text{S3.9a})$$

$$\vec{\mathbf{F}}_{\text{Roll}} = 2m\omega_R (-\dot{r} \text{Cos}\theta \text{Cos}\phi + r\dot{\theta} \text{Sin}\theta \text{Cos}\phi + r\dot{\phi} \text{Cos}\theta \text{Sin}\phi) \hat{\mathbf{Y}} + 2m\omega_R (\dot{r} \text{Sin}\theta + r\dot{\theta} \text{Cos}\theta) \hat{\mathbf{P}} \quad (\text{S3.9b})$$

$$\vec{\mathbf{F}}_{\text{Yaw}} = 2m\omega_Y (\dot{r} \text{Cos}\theta \text{Cos}\phi - r\dot{\theta} \text{Sin}\theta \text{Cos}\phi - r\dot{\phi} \text{Cos}\theta \text{Sin}\phi) \hat{\mathbf{R}} + 2m\omega_Y (-\dot{r} \text{Cos}\theta \text{Sin}\phi + r\dot{\theta} \text{Sin}\theta \text{Sin}\phi - r\dot{\phi} \text{Cos}\theta \text{Cos}\phi) \hat{\mathbf{P}} \quad (\text{S3.9c})$$

To bring these terms back into spherical system, we substitute Equation S3.5 (a, b, c) to obtain:

$$\begin{aligned} \vec{\mathbf{F}}_{\text{Pitch}} = \hat{r}(-2m\omega_p r\dot{\theta} \text{Sin}\phi + 2m\omega_p r\dot{\phi} \text{Sin}\theta \text{Cos}\theta \text{Cos}\phi) \\ + \hat{\theta}(2m\omega_p \dot{r} \text{Sin}\phi + 2m\omega_p r\dot{\phi} \text{Cos}^2\theta \text{Cos}\phi) \\ + \hat{\phi}(2m\omega_p \dot{r} \text{Sin}\theta \text{Cos}\phi + 2m\omega_p r\dot{\theta} \text{Cos}\theta \text{Cos}\phi) \end{aligned} \quad (\text{S3.10a})$$

$$\begin{aligned} \vec{\mathbf{F}}_{\text{Roll}} = \hat{r}(2m\omega_R r\dot{\theta} \text{Cos}\phi + 2m\omega_R r\dot{\phi} \text{Sin}\theta \text{Cos}\theta \text{Sin}\phi) \\ + \hat{\theta}(-2m\omega_R \dot{r} \text{Cos}\phi + 2m\omega_R r\dot{\phi} \text{Cos}^2\theta \text{Sin}\phi) \\ + \hat{\phi}(2m\omega_R \dot{r} \text{Sin}\theta \text{Sin}\phi + 2m\omega_R r\dot{\theta} \text{Cos}\theta \text{Sin}\phi) \end{aligned} \quad (\text{S3.10b})$$

$$\begin{aligned} \vec{\mathbf{F}}_{\text{Yaw}} = \hat{r}(-2m\omega_Y r\dot{\phi} \text{Cos}^2\theta) \\ + \hat{\theta}(2m\omega_Y r\dot{\phi} \text{Cos}\theta \text{Sin}\theta) \\ + \hat{\phi}(-2m\omega_Y \dot{r} \text{Cos}\theta + 2m\omega_Y r\dot{\theta} \text{Sin}\theta) \end{aligned} \quad (\text{S3.10c})$$

Rearranging the above equation, the Coriolis force components in terms of r , θ , ϕ are

$$F_r = 2m [\omega_p(-r\dot{\theta} \sin \phi + r\dot{\phi} \sin \theta \cos \theta \cos \phi) + \omega_R(r\dot{\theta} \cos \phi + r\dot{\phi} \sin \theta \cos \theta \sin \phi) - \omega_Y(r\dot{\phi} \cos^2 \theta)] \quad (\text{S3.11a})$$

$$F_\theta = 2m [\omega_p(\dot{r} \sin \phi + r\dot{\phi} \cos^2 \theta \cos \phi) + \omega_R(-\dot{r} \cos \phi + r\dot{\phi} \cos^2 \theta \sin \phi) + \omega_Y(r\dot{\phi} \cos \theta \sin \theta)] \quad (\text{S3.11b})$$

$$F_\phi = 2m [\omega_p(\dot{r} \sin \theta \cos \phi + r\dot{\theta} \cos \theta \cos \phi) + \omega_R(\dot{r} \sin \theta \sin \phi + r\dot{\theta} \cos \theta \sin \phi) + \omega_Y(-\dot{r} \cos \theta + r\dot{\theta} \sin \theta)] \quad (\text{S3.11c})$$

These terms are relevant to the oscillating antenna and the underlying mechanosensory fields.

Approximations for the specific case of *Manduca sexta*

For the case of *Manduca sexta*, we make the following assumptions based on our experimental observations.

- 1) We assume \dot{r} to be negligible because to measurement resolution, r is constant in our studies. For simplicity, we have set the product $2mr$ to unity in the calculations below.
- 2) Because the moths hold their antenna at small θ, ϕ about which the antenna oscillates at wing beat frequency, the input to antenna is modeled as a sinusoid function of time.

From these considerations, the force equations simplify to:

$$F_\theta = \omega_p(\dot{\phi} \cos^2 \theta \cos \phi) + \omega_R(\dot{\phi} \cos^2 \theta \sin \phi) + \omega_Y(\dot{\phi} \cos \theta \sin \theta) \quad (\text{S3.12a})$$

$$F_\phi = \omega_p(\dot{\theta} \cos \theta \cos \phi) + \omega_R(\dot{\theta} \cos \theta \sin \phi) + \omega_Y(\dot{\theta} \sin \theta) \quad (\text{S3.12b})$$

Frequency response of forces

To determine the frequency response of the forces, we consider the special cases of pure pitch, pure roll and pure yaw. The peaks in the Fourier transform of the forces reveals the frequency response of the forces and consequent θ , ϕ deflections.

The sinusoidal motions along these angles are modeled using the following simple harmonic equations:

$$\theta(t) = \theta_o + \theta_{amp} \text{Sin}(2\pi nt) \quad (\text{S3.13a})$$

$$\phi(t) = \phi_o + \phi_{amp} \text{Sin}(2\pi nt) \quad (\text{S3.13b})$$

where θ_o , ϕ_o are the arbitrary fixed small angles at which the moths hold their antenna, and θ_{amp} , ϕ_{amp} are the conservative estimates for amplitudes of oscillation and n is the wing beat frequency. To a first approximation, we assume that $\theta(t)$ and $\phi(t)$ have the same kinematics in equations S3.13 (a, b).

Special Case 1: Pure Yaw

$$F_\theta = \omega_Y (\dot{\phi} \text{Cos} \theta \text{Sin} \theta) \quad (\text{S3.14a})$$

$$F_\phi = \omega_Y (\dot{\theta} \text{Sin} \theta) \quad (\text{S3.14b})$$

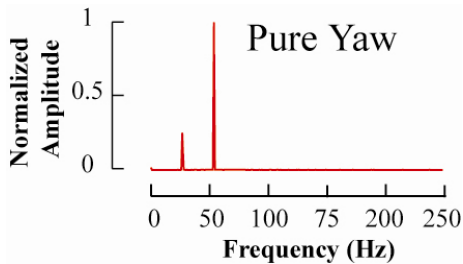


Figure S2: Fourier composition of Coriolis forces in pure yaw

Special Case 2: Pure Pitch

$$F_\theta = \omega_P (\dot{\phi} \text{Cos}^2 \theta \text{Cos} \phi) \quad (\text{S3.15a})$$

$$F_{\phi} = \omega_p (\dot{\theta} \cos \theta \cos \phi) \quad (\text{S3.15b})$$

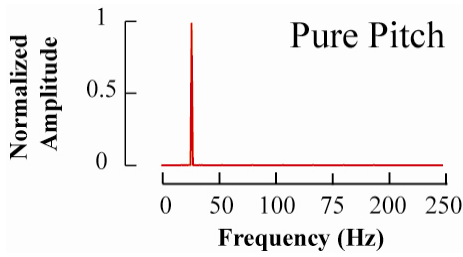


Figure S3: Fourier composition of Coriolis forces in pure pitch

Special Case 3: Pure Roll

$$F_{\theta} = \omega_R (\dot{\phi} \cos^2 \theta \sin \phi) \quad (\text{S3.16a})$$

$$F_{\phi} = \omega_R (\dot{\theta} \cos \theta \sin \phi) \quad (\text{S3.16b})$$

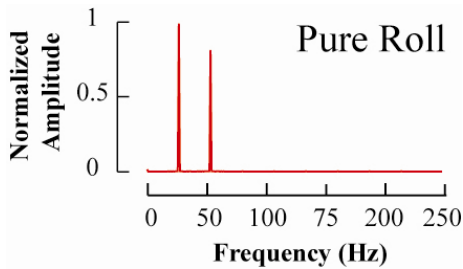


Figure S4: Fourier composition of Coriolis forces in pure roll

As evident from these plots, the first and second multiples of wing beat frequency are particularly relevant to the forces and the consequent deflections of the antennae. In the case shown here, yaw and roll maneuvers both show peaks at the first (27 Hz) and second (54 Hz) multiples of wing beat frequency, whereas pitch shows only a peak at wing beat frequency (27 Hz).

S4: Neurophysiology of antennal mechanosensors

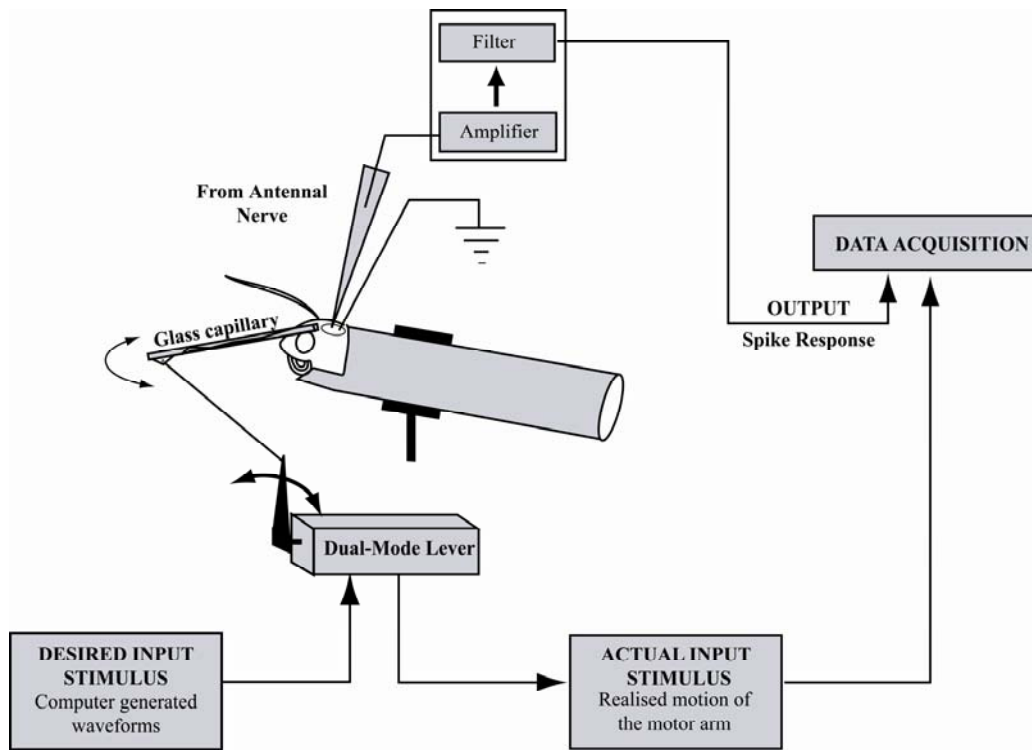


Figure S5: Schematic for intracellular recordings from antennal mechanosensors

During neurophysiology, we immobilized the moth by first inserting its thorax and abdomen in a plastic tube and restricting their motion with a mixture of beeswax and rosin. We attached the scape to the head capsule, and pedicel to the scape with wax. By inserting the moth's flagellum in a narrow glass capillary, we ensured that a bulk of antennal tip motion was transferred directly to the Johnston's organ *via* motion in the pedicel-flagellum joint. To gain access to the antennal nerve for intracellular recordings, we removed the dorsal part of the head capsule. The plastic tube enclosing the moth was then attached to a short metal pole mounted on a vibration free table.

To achieve fine control of the antennal motion, we used a 300B series dual-mode servo lever system (Aurora Scientific, Inc., Aurora, ON, Canada) and vibrated the

antennae along pre-programmed patterns using a MATLAB (The Mathworks Inc., Natick, NJ) custom graphical user interface (GUI). This GUI interfaced with an AD/DA device with multiple input/output channels and delivered the stimulus at 1 kHz. (National Instruments PCI MIO, 16E-4) attached to a BNC 2090 Adapter (National Instruments). The GUI simultaneously recorded the motion of the servo lever at 10 kHz thus tracking the actual mechanical stimulus to the antenna. The maximum displacement of the antenna due to the stimuli varied from experiment to experiment, typically ranging between 1° and 2.5°.

We obtained intracellular recordings from single axons in the antennal nerve using quartz electrodes (80-150 MΩ) filled with 0.1M KCl or LiCl solution. The raw signal was amplified by a factor of 10 using an intracellular amplifier (Neuroprobe Amplifier, A-M Systems Inc., Carlsborg, USA) and filtered using an off-line signal filter (Hum Bug, Quest Scientific, North Vancouver BC, Canada) to remove the ambient 60-cycle noise. The custom GUI recorded this data at 10 KHz and stored it for post-analysis. During an experiment or post-recording, we injected the neurons with the fluorescent dyes Alexa Fluor 568 or Lucifer Yellow (Molecular Probes, Inc., Eugene, OR) to visualize their projection patterns in the brain. After each experiment, the brain was dissected out and dehydrated through an ethanol series. The tissue was then cleared with methyl salicylate and imaged using a confocal microscope (Bio-Rad, MRC 2000). The images were reconstructed from planar confocal sections using NIH ImageJ software.

S5: Free flight behavior of moths with intact vs. amputated flagella.

Free flight behavioral experiments were carried out in a 0.9 X 0.9 X 0.6 m chamber illuminated by panel arrays of low power infra-red light emitting diodes. Because *Manduca sexta* is a crepuscular moth typically active under low light conditions, we darkened the chamber (maximum ambient luminosity = 1.3 lux) before filming except for a small light source to motivate the animals to fly. All experiments reported here were carried out on male *Manduca sexta*. Two orthogonal video cameras (Sony Digital8 DRC-TRV 310) on the Nightshot™ setting recorded the body trajectories at 30 fps. During post-processing, the films were played back at 10 frames per second to slow down the sequences for easier observation. The flight sequences were divided into several flight ‘bouts’. A bout was defined as a continuous flight sequence of from take-off to landing.

In all experiments, 2-3 day old moths were kept in a small dark chamber for 1-3 hours prior to the experiment. After the room was darkened in preparation for the flight tests, the moths were released in the flight chamber. Moths typically initiated warm-up within 5 minutes of their introduction into the flight chamber and began flying immediately afterward.

In the first set of experiments involving moths with intact vs. amputated flagella, we allowed the moths to fly in the chamber several minutes before filming their ‘control flight’ (S6). After filming of control flight, we waited for the moth to land on the wall of the chamber and quickly clipped off the antennae with a pair of micro-dissection scissors. Because these moths were already warm from previous bouts of flight, they could initiate flight immediately after their flagella were removed (S7). In some cases for both experimental and antennectomized moths, if the moths did not fly spontaneously

following warm-up, flight was initiated by lightly tapping a pen on the wall or floor of the cage.

In the second set of experiments, moths were cold anesthetized by keeping them in a -4°C chamber until their activity was diminished. These moths were constantly monitored during the cold anesthesia. Once a moth had ceased activity, they were kept in the chamber for an additional minute. The cold anesthetized moths typically stayed inactive for 5 minutes before resuming activity. We completed the surgical detachment and reattachment within this time window. As in the first experiment, the moth's antennae were clipped at the base (<10 annuli from the pedicel-flagellar joint) and immediately reattached to the stub with cyanoacrylate glue. The moths were then allowed to recover from surgery in the small dark chamber for about 1 hour. Thereafter, the experimental procedure was similar to the first set of experiments.

The main defects in flight sequences of the moths with amputated flagella were divided into three distinct subjective categories (see supplementary video *S7* for examples of these categories): (1) Collisions: When moths with amputated flagella take-off, they are often unable to finely adjust their body orientation resulting in sudden and uncontrolled acceleration towards the walls of the flight chamber, ultimately resulting in a 'collision'. Shortly after a collision, the moths often collided with other walls as they tried to regain control of their flight trajectory. (2) Crashes: A subset of the collisions led to complete failure of flight and 'crashes' to the floor. In a few cases, crashes also occurred without collisions. (3) Backwards Flight: Moths with amputated flagella were often unable to control their heading resulting in 'backwards' flight. Although these three categories are not mutually exclusive, each is indicative of specific abnormality with

flight. In all, we analyzed 491 bouts totaling approximately 67 minutes of flight. For experiments with moths with normal flagella (control) vs. moths with amputated flagella (n=10), we analyzed 69 flight bouts for control moths (S6, 6.9 bouts/ moth, mean bout time=23.2 ± 13.4 secs) and 166 bouts for moths with amputated flagella (S7, 16.6 bouts / moth, mean bout time=5.7 ± 2.1 secs). For experiments with moths with reattached flagella vs. moths with reamputated flagella (n=7), we analyzed 134 bouts of moths (S8, 19.1 bouts/moth, mean bout time=9.6 ± 8.5 secs) with reattached flagella, 122 bouts of moths with reamputated flagella antennae (17.4 bouts/ moth, mean bout time=3.6 ± 1.9 secs).

Supplementary videos of flight performance of moths:

All videos were recorded at 30 frames per second and played at 10 frames per second.

(S6) Moth with intact flagella,

(S7) Moths with removed flagella and

(S8) Moths with flagella reattached with glue

References

1. S. Vogel, *Life in Moving Fluids: The Physical Biology of Flow* (Princeton University Press, Princeton, New Jersey, ed. Second, 1994) pp 336.
2. White, F.M. (1974) *Viscous Fluid Flow* New York, NY McGraw-Hill
3. Unpublished data, MA Willis.
4. S. P. Sane, N. P. Jacobson, *J. Exp. Biol.* **209**, 43-56 (2006).